

Learning Representative Trajectories of Dynamical Systems via Domain-Adaptive Imitation

Edgardo Solano-Carrillo

EDGARDO.SOLANOCARRILLO@DLR.DE

Jannis Stoppe

JANNIS.STOPPE@DLR.DE

German Aerospace Center (DLR)

Institute for the Protection of Maritime Infrastructures

Fischkai 1, 27572 Bremerhaven - Germany

Abstract

Domain-adaptive trajectory imitation is a skill that some predators learn for survival, by mapping dynamic information from one domain (their speed and steering direction) to a different domain (current position of the moving prey). An intelligent agent with this skill could be exploited for a diversity of tasks, including the recognition of abnormal motion in traffic once it has learned to imitate representative trajectories. Towards this direction, we propose DATI, a deep reinforcement learning agent designed for domain-adaptive trajectory imitation using a cycle-consistent generative adversarial method. Our experiments on a variety of synthetic families of reference trajectories show that DATI outperforms baseline methods for imitation learning and optimal control in this setting, keeping the same per-task hyperparameters. Its generalization to a real-world scenario is shown through the discovery of abnormal motion patterns in maritime traffic, opening the door for the use of deep reinforcement learning methods for spatially-unconstrained trajectory data mining.

1. Introduction

This paper is generally concerned with the problem of learning the distribution of trajectories generated by a dynamical system, when only partial information about its evolution rule is known. Such systems — evolving as $s_{t+1} = f(s_t)$, with $f : \mathbb{R}^d \rightarrow \mathbb{R}^d$ being an unknown *stochastic* function and s_0 having a known distribution — are ubiquitous in science and engineering; a reason why advances in their understanding (which are independent of their state representation) have the potential of impacting a number of research fields. Such a global understanding is one of the goals of this work, which we exemplify by developing a model for learning statistics of f that is benchmarked for a diversity of synthetic systems and then used (with slight modifications) in a real-world scenario with a completely different state representation and geometry.

The starting point for our analysis is recognizing that the state of the system $s_t \in \mathbb{R}^d$ and the representation $\hat{a}_t \in \mathbb{R}^m$ of the partial knowledge of its evolution rule belong to two different geometric manifolds, \mathcal{S} and \mathcal{A} , respectively. These are connected by a known *deterministic* function $g : \mathcal{S} \times \mathcal{A} \rightarrow \mathcal{S}$ defining such a knowledge, in a way that makes $\hat{s}_{t+1} = g(\hat{s}_t, \hat{a}_t)$ approximate the state s_{t+1} at each time step. In our formulation, the stochasticity of f is taken on by the random variables \hat{a}_t and, since g is not necessarily bilinear, a wide range of systems may be considered. By observing an ensemble of sequences $s_{0:t}$ of states, our interest is then to learn the distribution of the corresponding sequences of *decision* variables $\hat{a}_{0:t}$ that generate the evolution of such states.

An example of the meaning of such formulation is provided by a cheetah learning to chase gazelles. In a given trial, the cheetah has to decide — from a snapshot of the current position s_t of the gazelle — the velocity vector \hat{a}_t making its position \hat{s}_t follow s_t as close as possible. Certainly, after many trials, the cheetah learns how to infer \hat{a}_t from complex environmental cues, after crucially discovering simple kinematics laws encapsulated by g . We refer to this learning process as *domain-adaptive trajectory imitation*, since it involves learning from a distribution of trajectories $s_{0:t}$ of a dynamical system, by adapting information from one domain \mathcal{A} to a different one \mathcal{S} , using partial knowledge of the evolution of s_t encoded by g . Since this task engages a decision maker, our approach is suitable for deep reinforcement learning methods (Lazaridis et al., 2020).

Although the ideas developed here may be extended to any dynamical system, we are motivated by a concrete practical application: *the detection of anomalies from real-time tracking data*. In particular, the results in this paper lead to a source of information for anomaly detection in maritime traffic that is alternative to the one that we have already exploited from a computer vision perspective (Solano-Carrillo et al., 2021), and then of great potential for maritime situational awareness. It may be useful in the detection of motion patterns corresponding to illegal activities, close in spirit with using agent-based simulations to match the empirical spatio-temporal distribution of crime locations from large-scale human activity data (Roses et al., 2020). Our approach is principled: detecting abnormal behavior by first *learning the distribution* of what is considered normal behavior and then measuring deviations from this at inference time. For this reason, it may be applied to time series featuring different characteristics (e.g., non-stationarity, irregular sampling rate, missing points, etc.) for which a plethora of different methods have been proposed per characteristic (Freeman et al., 2022).

Our key contributions in this paper are therefore:

- We introduce an OpenAI Gym environment (Brockman et al., 2016) supporting arbitrary families of reference trajectories (i.e. solutions to the mechanics of abstract dynamical systems) for the trajectory imitation problem. Four built-in families are provided for benchmarking existing and new learning methods;
- We propose a robust method (DATI) for learning representative trajectories of dynamical systems by framing the trajectory imitation task as a *reinforced* style transfer problem from the reference trajectories to the rollouts of the reinforcement learning agent – inspired by image to image translation (Zhu et al., 2017);
- We explore, for the first time, the application of deep reinforcement learning for spatially-unconstrained trajectory data mining; in particular, anomaly detection from tracking data, using maritime traffic as a testbed.

The presentation of this work is structured in such a way as to highlight how a single model can learn the main statistical properties of a variety of dynamical systems: from synthetic to a real-world application, keeping (nearly) the same architecture and hyperparameters.

2. Related work

Since the work on dynamical systems is vastly represented in many research fields, here we restrict only to recent methodologies which inspire our present viewpoint.

Motion imitation. At the core of our approach is the acquisition of locomotive skills by an agent that learns to imitate motion. There has recently been increasing interest on this. Haarnoja et al. (2019) taught a robot how to walk from scratch with minimal per-task hyperparameter tuning and a modest number of trials to learn. A similar task was carried out by a drone learning how to fly to a goal marker (Becker-Ehmck et al., 2020). More agile locomotion skills have been learned by imitating (from video motion capture) animals (Peng et al., 2020), complex human acrobatics (Peng et al., 2018), basketball dribbling (Liu & Hodgins, 2018); and by simulating realistic human motion from a model of the muscle contraction dynamics (Lee et al., 2019). The above methods use agents with a fixed embodiment. Hafner et al. (2020) have proposed a learning framework for core locomotive skills that work for wide variety of legged robots keeping hyperparameter setting and reward scheme. More aligned with our domain-adaptive approach is learning from experts which are different from the agents due to a mismatch of viewpoint, morphology or dynamics (Raychaudhuri et al., 2021; Kim et al., 2020). Nevertheless, none of these methods deal with the problem of imitating center-of-mass trajectories with significant spatiotemporal extension and complex shapes, as we pursue in this paper.

Trajectory control. The problem of making a vehicle follow a pre-defined path in space is mainly approached in two ways: trajectory tracking (Lee & Kim, 2017), which demands tracking a timed reference signal; and path following (Rubi et al., 2020), where the time dependency is removed and only the geometry is considered. Applications are mostly found in the control of multicopter unmanned aerial vehicles; although moving object grasping is of interest to realize intelligent industrial assembly lines (Chen & Lu, 2021). Using learning-based methods, these applications include adapting the popular DDPG reinforcement learning method (Lillicrap et al., 2016) for solving the path following problem in a quadrotor with adaptive velocity and considering obstacle avoidance (Rubi et al., 2021a, 2021b). On the other hand, several inverse reinforcement learning approaches have been designed for tracking control (Xue et al., 2021a, 2021b). Our work is closer in spirit to Choi et al., 2017, where a representative trajectory is extracted from demonstrations and a reward function learned to imitate such trajectory. We train an agent to directly generate the representative trajectories (not necessarily observed in the training set) without learning a reward function though.

Trajectory data mining. The aim is to automatically discover interesting knowledge from trajectory datasets, which are typically generated from social, traffic, and operational dynamics (Wang et al., 2020a). Traditional clustering and classification methods have served as the basis for more in depth pattern mining and anomaly detection. For pattern mining, different methods have been used for different kinds of patterns, such as periodic (Li et al., 2010, 2012), frequent (Giannotti et al., 2006, 2007), and collective patterns (Zheng, 2015). For anomaly detection, the techniques are often based on clustering methods and its extensions (Belhadi et al., 2020); although supervised learning approaches have also been considered (Meng et al., 2019). The use of reinforcement learning for anomaly detection has mainly focused on road traffic (Oh & Iyengar, 2019), for which the motion

is constrained by the road networks. In a spatially-unconstrained context, such as the maritime traffic, the trajectory shape complexity increases, encouraging the use of computer vision for trajectory classification (Kontopoulos et al., 2021), or graph methods for the detection of representative trajectories (Zygouras et al., 2021). We contribute with a novel deep reinforcement learning method capable of discovering both periodic and non-periodic patterns in spatially-unconstrained trajectory data using a single model.

We emphasize here that, although our work is aligned in objectives with the solution of the problem of motion imitation and trajectory control, we are not interested on the design of controllers allowing a safe navigation of an embodied agent (e.g. autonomous vehicle) under uncertain environments. This requires a model of the inertial properties of the vehicles and their interactions with the environments. We rather aim at a disembodied agent which learns to imitate the typical patterns in traffic to then be able to tell the atypical ones.

3. Background

In the following, we formulate the learning problem, describe how it can be reframed within the traditional imitation learning and optimal control settings, and introduce DATI in the next section as a novel method to solve the problem.

3.1 Preliminary

The evolution $s_{t+1} = f(s_t)$ of complex dynamical systems from an initial state s_0 is often hard to estimate. The difficulty lies in: 1) our ignorance of their intricate underlying mechanics, and 2) our ignorance of the nature of the noise source. We are interested in learning the joint distribution, p , of trajectories $s_{0:t} \equiv (s_0, s_1, \dots, s_t)$ of a dynamical system, provided we have knowledge of a local approximation to the underlying evolution rule. This is expressed by a deterministic decomposition of the update rule, $\hat{s}_{t+1} = g(\hat{s}_t, \hat{a}_t)$, in terms of random decision variables \hat{a}_t . Restricting our focus to Markovian processes, the joint distribution (assumed absolutely continuous and then admitting density¹) can be written as

$$p(s_{0:T}) = p_0(s_0) \prod_{t=0}^{T-1} p_t(s_{t+1}|s_t), \quad (1)$$

and the main task is learning how to sample from the *unknown* $p_t(s_{t+1}|s_t)$. Since knowledge of s_t and the true action a_t imply knowledge of s_{t+1} with complete certainty (by means of g), the task is equivalent to estimating $p_t(a_t|s_t)$. This is pursued by optimizing a policy (neural network) $\pi_{\vec{\theta}}(\hat{s}_t) \rightarrow \hat{a}_t$ which samples actions from the distribution $p_{\theta}(\hat{a}_t|\hat{s}_t, t)$, and from which the next state is approximated as $\hat{s}_{t+1} = g(\hat{s}_t, \pi_{\vec{\theta}}(\hat{s}_t)) \equiv \pi_{\theta}(\hat{s}_t)$. This optimization brings $p_{\theta}(\hat{a}_t|\hat{s}_t, t)$ close to $p_t(a_t|s_t)$ with respect to some distance/divergence discussed later.

3.2 Problem formulation

Given an ensemble of trajectories $s_{0:T} \sim p$ generated by a dynamical system, the task is to find a policy π_{θ} that replicates the shape of a *typical* trajectory $s_{0:T}^*$ after rolling out

1. We implicitly assume the support of all distributions to be divided into a grid with small cell size implied in practice by ε in definition 3.1. Notations such as $p_0(s_0)$ then refer to the probability that the initial state is in a cell containing s_0 .

$\pi_\theta(\hat{s}_t) \rightarrow \hat{s}_{t+1}$. That is, consider a partition of the time interval $[0, T]$ into τ equally-spaced timesteps.² Then, the predicted sequence $\hat{s}_{0:T}^\theta \equiv (\hat{s}_0, \pi_\theta(\hat{s}_0), \dots, \pi_\theta(\hat{s}_{T-1}))$ and the reference sequence $s_{0:T}^* \equiv (s_0^*, s_1^*, \dots, s_T^*)$, having the same starting state $\hat{s}_0 = s_0^*$, should match their shapes at optimal $\hat{\theta}$. For concreteness, the shape similarity is with respect to the dynamic time warping distance (Salvador & Chan, 2004) — popular for comparing two time series not necessarily aligned in time — so the optimal model has

$$\hat{\theta} = \arg \min_{\theta} D_{\text{dtw}}(\hat{s}_{0:T}^\theta, s_{0:T}^*). \quad (2)$$

In practice, n reference trajectories $s_{0:T}^*$ not seen during training of π_θ are sampled from p at inference time, and policies trained with n different seeds are rolled out from the corresponding initial conditions. This leads to our notion of typicality, and hence of a learned representative trajectory:

Definition 3.1 (Representative trajectory). Given a small $\varepsilon > 0$, a representative trajectory $\hat{s}_{0:T}^\theta$ is said to be learned by a policy π_θ if there is a reference trajectory $s_{0:T}^*$ (out of the n in the test set) for which $D_{\text{dtw}}(\hat{s}_{0:T}^\theta, s_{0:T}^*) < \varepsilon$.

Since we will be discussing different methods to bring $\hat{p}_t(\hat{a}_t|\hat{s}_t)$ close to $p_t(a_t|s_t)$, as mentioned in 3.1, our optimization objective in (2) is chosen as a common metric to compare these methods. In the following, we focus on a simple 2D representation of the state s_t ($d = 2$), as a proof of concept. This allows us to design an intuitive scenario similar to the cheetah chasing a gazelle but which does not end after predation.

3.3 Mouse and hidden cheese game

As a prototype for our synthetic experiments in section 5, consider a mouse (agent) chasing intermittently-hidden cheese (trajectory demonstrator). At timestep t , the mouse has to decide and act $\hat{a}_t = (u_t, \xi_t)$ to make its speed u_t and steering direction ξ_t to take it from its current position \hat{s}_t to the currently *unknown* position of the cheese. The latter is only revealed at timestep $t + 1$ to be $s_{t+1} \equiv (x_{t+1}, y_{t+1})$, and the mouse is perfectly rewarded if

$$s_{t+1} = g(\hat{s}_t, \hat{a}_t) \equiv \hat{s}_t + (u_t \cos(\xi_t), u_t \sin(\xi_t)) dt, \quad (3)$$

making it is able to taste the cheese (here $dt = T/\tau$). The second equality in (3) defines \hat{s}_{t+1} , so the cheese is tasted when $\hat{s}_{t+1} = s_{t+1}$. Since \hat{s}_t is stochastically generated, it is unlikely that this takes place, unless we impose a minimal distance between \hat{s}_t and s_t (e.g., being within the same cell, as mentioned in footnote 1) within which tasting really happens. In practice, this is implied by the selection of ε in definition 3.1.

The function g in this case represents an intuition about kinematics that the mouse has in advance. It is based only on partial information about the true evolution rule prescribed by $s_{t+1} = f(s_t)$, namely, an $O(dt)$ approximation, with a two-dimensional decision space \mathcal{A} . A different decomposition is obtained with an $O(dt^2)$ approximation, introducing accelerations as part of the decision variables \hat{a}_t . Note that a different geometry of the state space may also be considered, as in Eq. (8), or even problems not defining physical motion.

2. This assumption may be relaxed for real-world applications with irregular sampling rate of the data and varying horizons T , as in section 6.

The degree to which the decision variables \hat{a}_t (implied by a given decomposition) lead to a satisfactory replication of the shape of reference trajectories leads to the concept of a perfect decision maker:

Definition 3.2 (Perfect policy). Given a reference trajectory $s_{0:T}^*$, a perfect policy rollout $\pi^*(\hat{s}_t) \rightarrow \hat{s}_{t+1}$ replicates this trajectory indentially, by means of Eq. (3). That is, $\hat{s}_t = s_t^*, \forall t$, making $D_{\text{dtw}}(\hat{s}_{0:t}^\theta, s_{0:t}^*) = 0$. This means that the agent has full knowledge of the underlying mechanics of the process, guessing the next state, s_{t+1} , and taking corresponding actions $a_t = (u_t, \xi_t)$ with speed $u_t = \|s_{t+1} - s_t\|/dt$ and steering angle $\xi_t = \tan^{-1}[(s_{t+1} - s_t) \cdot \hat{y} / (s_{t+1} - s_t) \cdot \hat{x}]$ in order to get there.

Since life is not perfect, the ever hungry and intelligent mouse will learn, after many trials (containing similarly shaped $s_{0:T}$), to discover the main features of the cheese trajectories. At inference, the mouse is fooled with no cheese signal, but its trajectory is collected and compared with the reference $s_{0:T}^*$ to judge how representative it is. In the following, we describe different approaches that we will compare later for the solution of this problem.

3.4 Imitation learning

Imitation learning aims to learn a policy $\pi_\theta^{il}(s_t) \rightarrow \hat{a}_t$ mimicking demonstrations $\mathcal{D} = ((s_0, a_0), (s_1, a_1), \dots, (s_T, a_T))$ from an expert whose actions $a_t \sim \pi^*$ are collected after observation of many instances of environmental state sequences $s_{0:T}$. Several approaches have been developed for this, see e.g. Zheng et al. (2021) for a survey. The simplest baseline, which we adopt here for benchmarking the synthetic experiments, is *Behavioral Cloning* (BC). This learns the policy by considering the setting as a supervised regression problem over \mathcal{D} (Pomerleau, 1991; Ross & Bagnell, 2010). That is, the unknown transition distribution $p_t(a_t|s_t)$ of relevance for (1) is estimated as $p_\theta(\hat{a}_t|s_t)$ after minimizing the Kullback-Leibler divergence between the two. This amounts to a maximum likelihood optimization of $p_\theta(\hat{a}_t|s_t)$.

The application of these method to the present problem demands the interpretation of the environment states s_t as comprising the trajectories $s_{0:T}$ to be imitated. The actions a_t in the demonstration set \mathcal{D} are generated by the best expert: a perfect policy π^* , according to definition (3.2). At inference, when the observations $s_{0:t}$ are removed, the predicted \hat{s}_t 's are used instead when rolling out the learned policy, i.e. $\hat{s}_{t+1} = g(\hat{s}_t, \pi_\theta^{il}(\hat{s}_t)) = \pi_\theta(\hat{s}_t)$.

3.5 Reinforcement learning using sparse rewards

In the standard reinforcement learning framework, the agent-environment interaction is modeled as a Markov decision process $(\mathcal{S}, \mathcal{A}, \mathcal{P}, r, \gamma, p_0)$, where \mathcal{S} and \mathcal{A} are the state and action spaces, respectively, $\mathcal{P}(s'|a, s)$ is the transition distribution of the environment, $r = r(s, a)$ is the reward function, $\gamma \in (0, 1)$ is the discount factor, and $p_0 = p_0(s)$ is the initial state distribution of the environment.

As a motivation behind our method, we adapt the DDPG agent (Lillicrap et al., 2016) to the trajectory imitation problem (denoted as DDPG-TI). This still consists of two actor-critic models — the learned $(\pi_\theta^l, c_{\theta_c}^l)$ and target $(\pi_\beta^r, c_{\beta_c}^r)$ networks, the latter slowly tracking the former during training — the actors guided by the return $R_t = \sum_{i=t}^T \gamma^{i-t} r(s_i, a_i)$ from a state. However, instead of having tuples (s_t, a_t, r_t, s_{t+1}) in the replay buffer during maximization of the expected return from the starting distribution, we use $(\hat{s}_t, \hat{a}_t, r_t, \hat{s}_{t+1}, t)$, where t is

processed by a scale-invariant embedding of time (Kazemi et al., 2019) which is shared by the networks. The reward signal here is $r_t = \pm 1$ according to whether or not $\tilde{D}_{\text{dtw}}(\hat{s}_{0:t}^\theta, s_{0:t}) < \varepsilon$, where the tilde denotes an exponentially-smoothed and normalized dynamic time warping distance. This is inspired by the constant rewards used by Reddy et al. (2020).

In this formulation, the agent does not make decisions \hat{a}_t during training based on the current state s_t , but rather on its current prediction of that state \hat{s}_t . This change is necessary to avoid the DDPG-TI agent taking the same actions regardless of the current state, an observation from early experimentation which motivated the introduction of the embedding of time. At inference, the learned policy leads to the predictions $\hat{s}_{t+1} = g(\hat{s}_t, \pi_\theta^l(\hat{s}_t, t) + \eta_t) = \pi_\theta(\hat{s}_t)$, where η_t is the noise used for exploration of the environment (originally taken as an Ornstein-Uhlenbeck process by Lillicrap et al., 2016).

4. Domain-adaptive trajectory imitation

Since we are interested in learning the distribution of the trajectories to be imitated, adding the noise η_t to the output of the actor entails a fake stochasticity in the results. So, building from DDPG-TI, the first observation is to change the actor $\pi_\theta^l(\hat{s}_t, t) \rightarrow \hat{a}_t + \eta_t$ to the actor $\pi_\theta^r(\hat{s}_t, \eta_t, t) \rightarrow \hat{a}_t$, taking us to the realm of generative models; in particular, the adversarial generative models (GANs) which recover the data distribution (Goodfellow, 2017).

With the above observation in mind, the main idea behind DATI may be informally stated as considering the imitation of $s_{0:t}$ by $\hat{s}_{0:t}$ as a *style* transfer problem between the domains spanned by these set of trajectories. Cycle-consistent generative adversarial networks (CycleGAN) (Zhu et al., 2017) have shown significant success in the style transfer task for unpaired image-to-image translation, so we extend them here to the domain-adaptive trajectory imitation problem, adding a novel reinforcement signal.

As with DDPG-TI, we have two actor-critic networks: $(\pi_\theta^r, c_{\theta_c}^r)$ and $(\pi_\beta^r, c_{\beta_c}^r)$. However, each pair is now trained adversarially using the Wasserstein loss (Arjovsky et al., 2017). Specifically, for the first pair, we take an actor $\pi_\theta^r(\hat{s}_t, \eta_t, t) \rightarrow \hat{a}_t$ which learns how to sample from the distribution $p_\theta(\hat{a}_t | \hat{s}_t, t)$ (sometimes just denoted $\hat{p}_t(\hat{a}_t | \hat{s}_t)$) by accessing the noise prior p_{η_t} . This is accomplished by valuing the chosen decisions with a critic $c_{\theta_c}^r(\hat{a}_t, r_t, t)$ — lying in the space of 1-Lipschitz functions³ (denoted $\|c_{\theta_c}^r\|_L \leq 1$), and r_t being the sparse rewards of section 3.5 — and both networks optimized as

$$\begin{aligned} \max_{\|c_{\theta_c}^r\|_L \leq 1} \mathbb{E}_{a_t \sim p_t(a_t | s_t)} [c_{\theta_c}^r(a_t)] - \mathbb{E}_{\eta_t \sim p_{\eta_t}} [c_{\theta_c}^r(\pi_\theta^r(\eta_t))], \\ \max_{\pi_\theta^r} \mathbb{E}_{\eta_t \sim p_{\eta_t}} c_{\theta_c}^r(\pi_\theta^r(\eta_t)), \end{aligned} \tag{4}$$

where we have omitted some arguments of the functions for simplicity. That is, the actor is trained to maximize the value that the critic assigns to its decisions (bottom of (4)), whereas the critic is trained to separate this value from the value of perfect decisions (top of (4)). These perfect decisions, a_t , are those from a perfect policy π^* according to definition 3.2.

This optimization procedure guarantees — under plausible continuity assumptions for the actor — that the distribution $p_\theta(\hat{a}_t | \hat{s}_t, t)$ converges to the true distribution $p_t(a_t | s_t)$ with respect to the Wasserstein (a.k.a Earth Mover) distance (Arjovsky et al., 2017). As

3. In our experiments, this condition is kept by adopting the method from Gulrajani et al. (2017).

mentioned, knowing the true a_t reproduces the next state as $s_{t+1} = g(s_t, a_t)$, so the $p_t(a_t|s_t)$ estimated by DATI through $p_\theta(\hat{a}_t|\hat{s}_t, t)$ basically leads to an approximation of the $p_t(s_{t+1}|s_t)$ that are of interest in (1).

The networks in the second pair, $(\pi_\beta^\leftarrow, c_{\beta_c}^\leftarrow)$, have the same architecture as their respective networks in the first pair. However, the actor $\pi_\beta^\leftarrow(\hat{a}_t, \eta_t, t) \rightarrow \hat{s}_t^\leftarrow$ is concurrently trained to *undo* the action of $\pi_\theta^\rightarrow(\hat{s}_t, \eta_t, t) \rightarrow \hat{a}_t$, i.e. by reconstructing the \hat{s}_t that is targeted by \hat{s}_t^\leftarrow . This “backward” actor, π_β^\leftarrow , is valued by a critic $c_{\beta_c}^\leftarrow(\hat{s}_t^\leftarrow, r_t, t)$, both trained similar to (4)

$$\begin{aligned} \max_{\|c_{\beta_c}^\leftarrow\|_{L \leq 1}} \mathbb{E}_{\hat{s}_t \sim \hat{p}_t(\hat{s}_t|\hat{a}_t)} [c_{\beta_c}^\leftarrow(\hat{s}_t)] - \mathbb{E}_{\eta_t \sim p_{\eta_t}} [c_{\beta_c}^\leftarrow(\pi_\beta^\leftarrow(\eta_t))], \\ \max_{\pi_\beta^\leftarrow} \mathbb{E}_{\eta_t \sim p_{\eta_t}} c_{\beta_c}^\leftarrow(\pi_\beta^\leftarrow(\eta_t)), \end{aligned} \quad (5)$$

where samples from $\hat{p}_t(\hat{s}_t|\hat{a}_t)$ are obtained by rolling out the “forward” policy π_θ^\rightarrow . This requires further explanation, since we we have said in the previous paragraph that π_θ^\rightarrow samples from the distribution $\hat{p}_t(\hat{a}_t|\hat{s}_t)$, not the posterior $\hat{p}_t(\hat{s}_t|\hat{a}_t)$. The question is: if $\pi_\theta^\rightarrow(\cdot, \eta_t, t)$ maps \hat{s}_t deterministically into \hat{a}_t , is the value of \hat{s}_t implied by having only knowledge of \hat{a}_t (and, of course, of η_t, t)? The answer is yes, provided that $\pi_\theta^\rightarrow(\cdot, \eta_t, t)$ is a *bijective* mapping. Therefore, whenever a value of \hat{a}_t is fetched from the replay buffer — which collects the tuples $(\hat{s}_t, \hat{a}_t, a_t, r_t, \eta_t, t)$ — there is only one possible value of \hat{s}_t which produced that value of \hat{a}_t using π_θ^\rightarrow , namely, the one recorded in the same tuple.

The bijective nature of the actors π_θ^\rightarrow and π_β^\leftarrow is enforced using *cycle consistency*. That is, by making both $\pi_\beta^\leftarrow \circ \pi_\theta^\rightarrow$ and $\pi_\theta^\rightarrow \circ \pi_\beta^\leftarrow$ approximate the identity mapping:

$$\begin{aligned} \min_{\pi_\theta^\rightarrow, \pi_\beta^\leftarrow} \mathbb{E}_{\hat{a}_t \sim \hat{p}_t(\hat{a}_t|\hat{s}_t)} \|\pi_\theta^\rightarrow(\pi_\beta^\leftarrow(\hat{a}_t)) - \hat{a}_t\|_1, \\ \min_{\pi_\theta^\rightarrow, \pi_\beta^\leftarrow} \mathbb{E}_{\hat{s}_t \sim \hat{p}_t(\hat{s}_t|\hat{a}_t)} \|\pi_\beta^\leftarrow(\pi_\theta^\rightarrow(\hat{s}_t)) - \hat{s}_t\|_1. \end{aligned} \quad (6)$$

Note that the bottom of (6) is a statement of minimization of the reconstruction error $\|\hat{s}_t^\leftarrow - \hat{s}_t\|_1$: the output of π_β^\leftarrow is supervised by confronting it against the ground truth \hat{s}_t . To achieve a comparable supervision for π_θ^\rightarrow , we enforce its output \hat{a}_t to approximate the ground truth a_t via L_1 penalty:

$$\min_{\pi_\theta^\rightarrow} \mathbb{E}_{\hat{s}_t \sim \hat{p}_t(\hat{s}_t|\hat{a}_t), a_t \sim p_t(a_t|s_t)} \|\pi_\theta^\rightarrow(\hat{s}_t) - a_t\|_1, \quad (7)$$

with the real a_t ’s being obtained, as before, from a perfect policy π^* according to definition 3.2. At inference, the “forward” actor is used for the trajectory predictions according to $\hat{s}_{t+1} = g(\hat{s}_t, \pi_\theta^\rightarrow(\hat{s}_t, \eta_t, t)) = \pi_\theta(\hat{s}_t)$

Finally, the motivation for using the scale-invariant embedding of time by Kazemi et al. (2019) in our method is to obtain a positional encoding of the time series representing the trajectories which is able to capture both periodic and non-periodic patterns in the data, regardless of whether we use the index i of the time $t = i dt$ of each event. This will prove to be beneficial for our method from the ablation studies in section 5.2.

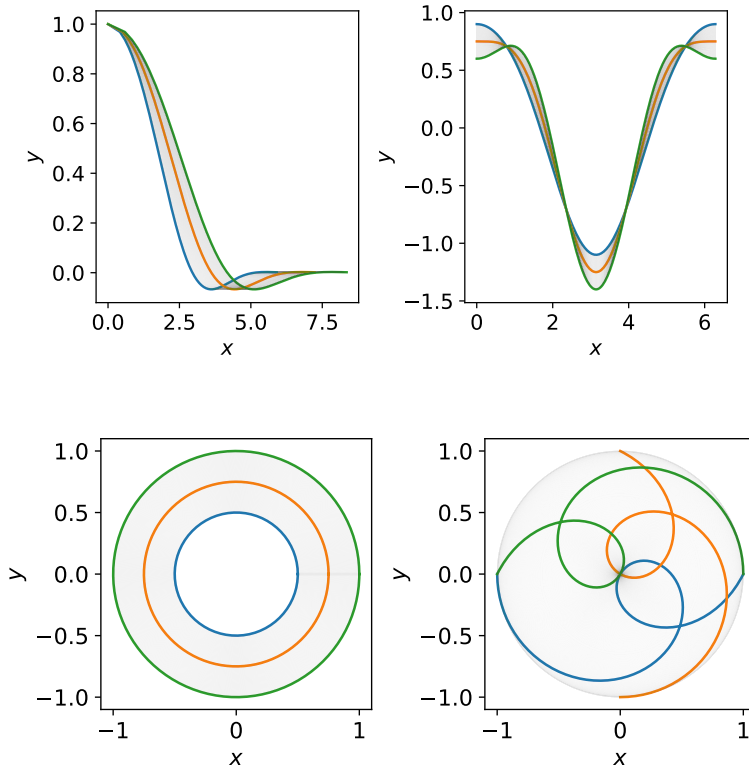


Figure 1: Family of trajectories \mathcal{F}_α considered for the domain-adaptive imitation task (from top left to bottom right: FixedStart, UShaped, Circles and Ribbons). These may be thought of as solutions to abstract dynamical systems with a two-dimensional state representation.

5. Synthetic experiments

The synthetic experiments are carried out on a variety of families of solutions to the mechanics of hypothetical dynamical systems. These are characterized by the initial state distribution $p_0(s_0)$ in (1), and a prescription to generate the subsequent states $s_{1:t}$ of the trajectory deterministically, given s_0 . The corresponding ensembles are denoted by \mathcal{F}_α : comprising a family of trajectories with shape parameters $\alpha = \{\alpha, \dots\}$ — all fixed except α , which is sampled uniformly within given intervals for each episode.

We provide an OpenAI Gym environment (Brockman et al., 2016) supporting (arbitrary) user-defined ensembles, \mathcal{F}_α , serving as demonstrations $s_{0:T}$ of the cheese signals for the mouse. We focus on four families defined in table 1 and visualized in Fig. 1:

1) *FixedStart* provides trajectories with the same starting point, having an inflection point near the beginning of the journey and then possibly confusing gradient descent methods aiming only at learning the mapping $x \rightarrow y$ (geometry without the time component).

2) *UShaped* provides trajectories with a reflection symmetry about a vertical axis passing through their lowest points, and having varying starting and ending features.

3) *Circles* provide the simplest expression of a periodic pattern in the trajectories. Nevertheless, they are complex enough, since the agents must keep their speed constant.

Family \mathcal{F}_α	$s_t = (x_t, y_t)$	
	x_t	y_t
FixedStart	$\sqrt{\alpha t}$	$\cos(\omega t) e^{-\kappa t}$
UShaped	ωt	$\cos(\omega t) - \alpha \cos(2\omega t)/2$
Circles	$\alpha \cos(\omega t)$	$\alpha \sin(\omega t)$
Ribbons	$R_1 - R_2 \cos(\omega t/4)$ $\times \cos(\omega t + \alpha)$	$R_1 - R_2 \cos(\omega t/4)$ $\times \sin(\omega t + \alpha)$

Table 1: Defining equations for the ensembles of trajectories \mathcal{F}_α used for benchmarking models. For the fixed values of the shape parameters complementary to α , see appendix A.1.

4) *Ribbons* provide trajectories to test how the networks disentangle space and time: by presenting a point in space that is visited twice with different headings.

5.1 Experimental setup and results

The experiments are carried out targeting robustness of the models to the variation of the learning tasks. So we keep the same hyperparameters for all the families of trajectories. Additionally, we impose a limit in the number of transitions for the models to learn the requested task. That is, we sample 100 episodes (a trajectory from \mathcal{F}_α per episode), each with a number of $\tau = 200$ timesteps. Code is supplementary provided for reproducibility.

Architectures. The actor-critic models for DATI are multilayer perceptrons with feature extractors having 16 units, time embedding dimension of 76, and 4 hidden layers – before the network outputs – having 32 units each. The critic networks process the rewards $r_t \in \{-1, 1\}$ by tiling the input to have the dimensionality of the sum of all other extracted-feature dimensions, passing this to a dense layer with non-negative kernel constraints and concatenating the output with such other extracted features before entering the 4 hidden layers previous to the (elu-activated) network output. The novel idea behind is that this propagates through the critic networks the signal of having low output for negative rewards and high output for positive rewards. Finally, the latent dimension of η_t for the actors is 64.

DDPG-TI has similar actor-critic architectures, but since the actors do not include a latent dimension, an increase of the feature extractors to 80 units is needed for their 4 hidden units before the output to observe the same input dimensionality as DATI. On the other hand, BC is trained using the `imitation` library (Wang et al., 2020b). In order to get actor architectures comparable to DDPG-TI and DATI, feature extractors with 156 units are used (making up the time embedding + latent dimensions + 16), followed by 4 hidden layers of 32 units. For the maximum likelihood estimation of $p_\theta(\hat{a}_t|s_t)$, the latent features before the output of π_θ^{il} are linearly transformed to define the mean and diagonal covariance of a Gaussian distribution $p_\theta(\hat{a}_t|s_t)$ network. Hyperparameter selection for the different methods may be found in appendix A.2.

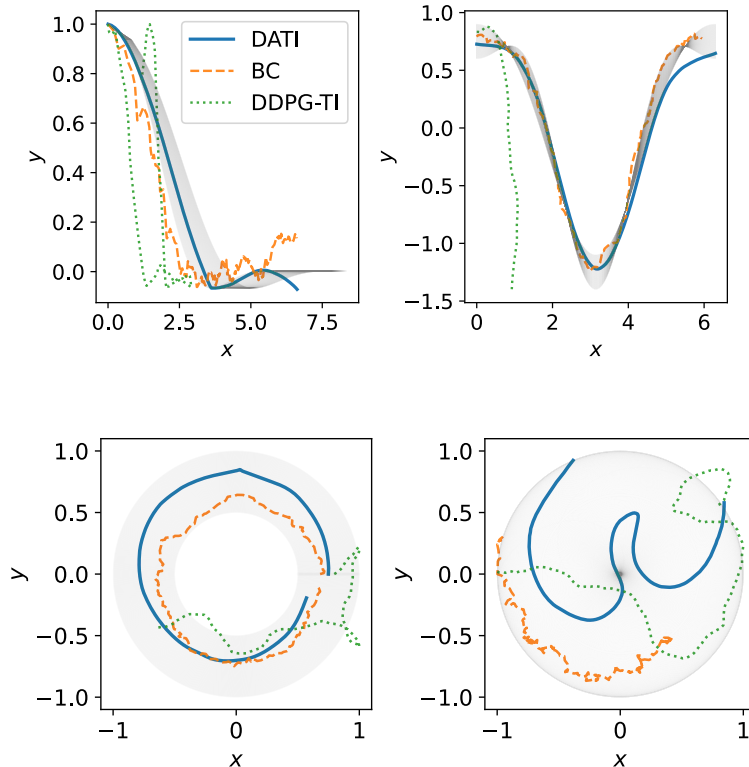


Figure 2: Rollouts $\pi_\theta(\hat{s}_t) \rightarrow \hat{s}_{t+1}$ of the learned policies for different methods at a seed giving the best dynamic time warping distance $\tilde{D}_{\text{dtw}}(\hat{s}_{0:T}^\theta, s_{0:T}^*)$ to a reference trajectory $s_{0:T}^*$ (with $\hat{s}_0 = s_0^*$), out of 10 trials. The results correspond, from top left to bottom right, to the families of trajectories \mathcal{F}_α with FixedStart, UShaped, Circles, and Ribbons of Fig. 1. For a quantitative assessment, see table 2.

Results. The models are trained with 10 seeds and evaluated with respect to 10 random reference trajectories s_t^* not seen in the training set. We compare the performance by reporting the best exponentially smoothed and normalized dynamic time warping distance $\tilde{D}_{\text{dtw}}(\hat{s}_{0:T}^\theta, s_{0:T}^*)$ over the 10 test trials. The normalization constant is the dynamic time warping “diameter” D_{dtw}^\gt , defined as the distance between the blue and green boundary trajectories in Fig. 1. The results are shown in table 2, with a visualization of the shapes of the best trajectories attained at inference in Fig. 2.

	FixedStart	UShaped	Circles	Ribbons
DDPG-TI	0.489	2.138	0.972	0.172
BC	0.124	0.365	0.106	0.113
DATI	0.065	0.231	0.058	0.033

Table 2: Lowest $\tilde{D}_{\text{dtw}}(\hat{s}_{0:T}^\theta, s_{0:T}^*)$ over 10 test trials.

Transformation	$\tilde{D}_{\text{dtw}}(\hat{s}_{0:T}^\theta, s_{0:T}^*)$	
	top-1	top-2
Original setup	0.058	0.074
No time embedding	1.829	1.976
No reward reinforcement	0.305	0.451

Table 3: Changes in the metric used in table 2 under ablation of some layers in the actor-critic models in DATI. The experiments are carried out for the family of Circles trajectories.

Clearly, DATI is able to generate trajectories that look closer to the ones in the families \mathcal{F}_α . Note that DATI and DDPG-TI were both trained using the reward signal $r_t = \pm 1$ according to whether or not $\tilde{D}_{\text{dtw}}(\hat{s}_{0:t}^\theta, s_{0:t}) < \varepsilon$. For the experiments, the ε in definition 3.1 is taken as 10% of the dynamic time warping diameter D_{dtw}^\gt . So only DATI is able to learn representative trajectories in most of the cases (numbers below 0.1 in table 2). We further investigate now the importance of some design choices in the actor-critic models in DATI.

5.2 Ablation study

We take the family of Circles trajectories and apply the following transformations — all other things being equal — to the architecture of the actor-critic models in DATI:

- *No time embedding*: we remove the notion of time exogenously imposed on the networks.
- *No reward reinforcement*: we do not let the critics know about the goal of minimizing the dynamic time warping distance between actor rollouts and demonstrations.

In order to get sensible statistical results (Agarwal et al., 2021) of the effect of these changes, it suffices to monitor the best and second best $\tilde{D}_{\text{dtw}}(\hat{s}_{0:T}^\theta, s_{0:T}^*)$ over the 10 test trials. These are shown in table 3. We observe a significant negative impact on the performance when the time embedding is removed. Similarly, removing the reward signal has appreciable negative effects. These are therefore essential ingredients in the design of DATI.

The conclusion from these experiments is that DATI is a successful method for learning representative trajectories, being robust to changes in their geometries — i.e. keeping the same architecture and hyperparameters it can represent a rich set of spatiotemporal phenomena. In order to further test this, we evaluate its generalization to a real world scenario, taking maritime traffic as an example.

6. Real-world experiments

We consider vessel traffic between the surroundings of Miami and the entrance to the gulf of Mexico in 2015 (UTM zone 17). The dataset for this is publicly available,⁴ the variables of interest being the longitude (λ), the latitude (φ), the speed over ground (SOG), the course over ground (COG), and the timestamp of every AIS signal reported by vessels moving with $\text{SOG} > 3$ knots. We filter out some of the trajectories going to or coming from the

4. <https://marinecadastre.gov/AIS/>.

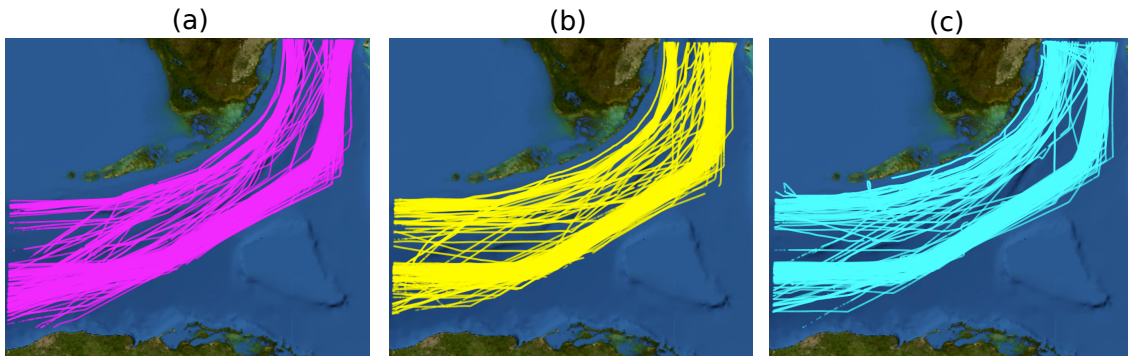


Figure 3: Vessel traffic of interest between the Miami surroundings (north east) and the entrance to the gulf of Mexico (south west) in 2015. (a) trajectories always going up (b) trajectories always going down (c) rest of the trajectories.

eastern Greater Antilles as well as on the north of the Florida Keys. From the remainder, we keep trajectories which have at least 900 timesteps, leaving a dataset of about 3.2M records extracted from a totality of about 36.5M records. This is clustered into 3 categories: trajectories always going *up* ($-90^\circ \leq \text{COG} \leq 90^\circ$), trajectories always going *down*, and the rest of the trajectories in *other*. These are partially shown in Fig. 3, after removal of outliers (Young, 2017) and segmentation at stop points (Bay, 2017) of more than an hour. They fit inside a region of interest (ROI) whose boundary is clearly appreciable from Fig. 3.

6.1 Partial knowledge about the update rule

The motion of vessels is spatially-unconstrained, giving rise to maneuvers that are not seen on road traffic. Moreover, it occurs on a curved geometry and the reported dt is stochastic (Last et al., 2014). Nevertheless, it is our general goal to include a partial knowledge of the update rule into the models. This is obtained by approximating the motion on the surface of the Earth as (see appendix A.3 for details)

$$\begin{aligned}\varphi_{t+1} &= \varphi_t + \frac{1}{60} \cos(\text{COG}_t) \text{SOG}_t dt, \\ \lambda_{t+1} &= \lambda_t + \frac{1}{60} \sin(\text{COG}_t) \text{SOG}_t dt / \cos(\varphi_t),\end{aligned}\tag{8}$$

provided dt (measured in hours) is small enough. Defining the state as $s_t = (\lambda_t, \varphi_t)$ and the actions targeted by the agent as $a_t = (\text{SOG}_t, \text{COG}_t, dt)$, the equations in (8) define the functions g_λ and g_φ representing the partial knowledge that the agent has about the evolution of the state to be imitated. Compared to the synthetic experiments, here the agent has the extra task to learn the distribution of dt for the next AIS record of a vessel to arrive.

6.2 Detection of abnormal motion patterns

We train DATI with the same architecture and hyperparameters as in the synthetic experiments (except that $\pi_{\vec{\theta}}$ now has three instead of two outputs). To define the train and test sets, we notice that the cluster of *up* trajectories has 170 in total, the cluster of *down* trajectories has 1973 in total, and the cluster of *other* trajectories has 887 in total. By definition, the

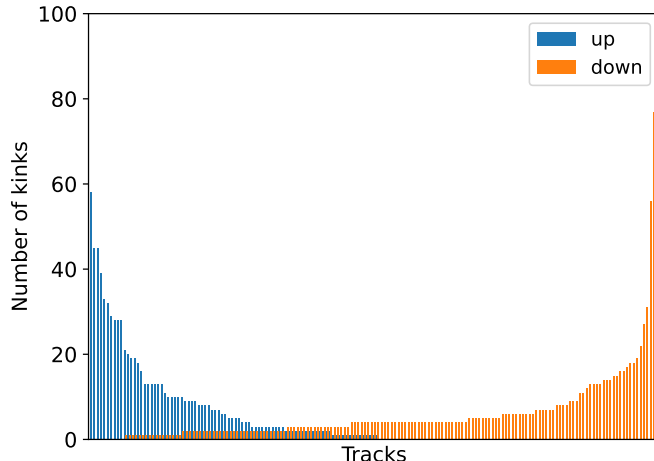


Figure 4: Number of course changes with $\Delta\text{COG} > 10^\circ$ (kinks) per track in the cluster *up* and in a uniformly sampled subset of 170 trajectories from the cluster *down*.

cluster *other* has trajectories which either go up or down but not monotonically, therefore having room for exotic vessel maneuvers. To discover abnormal motion, a subset of this cluster is then used as test set.

In order to have training conditions as in the synthetic experiments, we target a similar number of training episodes. For this reason, we take the whole cluster of *up* trajectories, giving 170 episodes, and downsample the cluster of *down* trajectories to also have 170 trajectories (the same is done for testing on the *other* cluster). These are the numbers shown in Fig. 3. Furthermore, to avoid the encoding of *up* and *down* as an extra feature of the state space, two DATI instances are trained, one for each cluster type.

The (exponentially-smoothed) dynamic time warping distance $D_{\text{dtw}}(\hat{s}_{0:T}^\theta, s_{0:T}^*)$ is now measured with respect to the great-circle distance on the surface of the Earth (unlike the Euclidean distance used for the synthetic experiments). Since the trajectories chosen for training comprise more than 300 km in length, we choose a relatively small $\varepsilon = 500$ m to reward DATI with $r_t = \pm 1$ according to whether $D_{\text{dtw}}(\hat{s}_{0:t}^\theta, s_{0:t}) < \varepsilon$ or not.

Probing the generated distribution. To make sense of how DATI conceives the data distribution, it is helpful to think of the main features that make up a vessel trajectory. Since there is an incentive to take the safest and shortest navigable route, trajectories may display many straight-line segments. We adopt a threshold for a significant change of course to be $\Delta\text{COG} = 10^\circ$, which we call a *kink*. Fig. 4 shows the amount of kinks in the train sets of both clusters. It is observed that the original cluster *down* is highly skewed toward trajectories with few kinks. The distribution is multimodal, with only 7% of the cluster not containing kinks, and 63% of the trajectories having from 1 to 4 kinks, in the proportion of 12%, 19%, 18%, and 13%, respectively. In contrast, 49% of the cluster *up* does not feature any kink, which means that the trajectories in this cluster are often smooth. It is then expected that these observations are reflected in the inductive biases of the learned models.

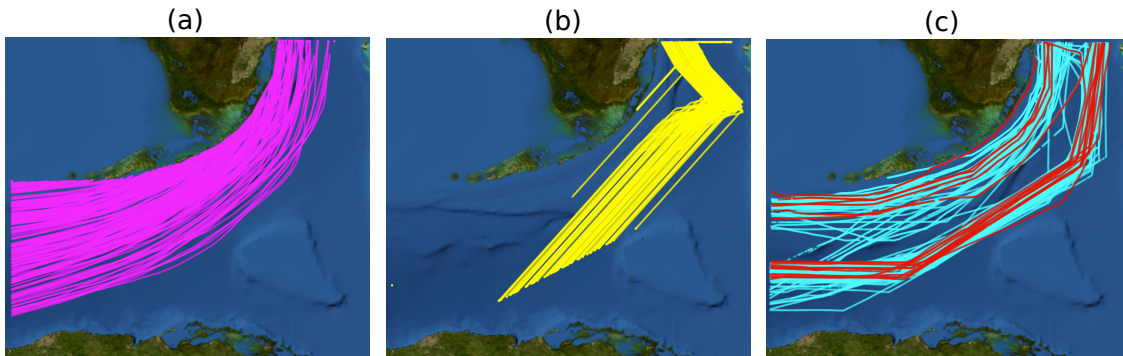


Figure 5: Trajectories generated by DATI after randomly sampling 170 initial states: (a) using the model trained with the cluster *up* (b) using the model trained with the cluster *down*. (c) Performance on the test set of trajectories that go up in the cluster *other*, showing corresponding anomalies identified by DATI (in red).

We rollout the learned policies starting from 170 random points along the vertical boundary at the entrance to the gulf of Mexico for the cluster *up* and along the horizontal boundary near Miami for the cluster *down*. The results are shown in Fig. 5(a)-(b). As expected, DATI learns to smoothly generate trajectories always going up, with shapes resampling the reference trajectories during training. It does so even in starting regions not observed during training, as can be seen by comparing Figs. 3(a) and 5(a). On the other hand, the model trained with the downsampled cluster of *down* trajectories learns to generate mainly 2 kinks from the most populated mode — this is different from the mode collapse sometimes encountered in GANs (Durall et al., 2021). However, in the attempt to fit the other types of trajectories, the end result does not resemble the shape of the trajectories observed during training, as seen by comparing Figs. 3(b) and 5(b). A solution for this may be found in downsampling this cluster not uniformly but by extracting much more smooth trajectories than with kinks.

An immediate observation from the generated trajectories is a sticking effect when the actors hit the boundaries of the ROI. This (i.e. $\hat{s}_{t+1} \rightarrow \hat{s}_t$ if $\hat{s}_{t+1} \notin \text{ROI}$) happens until the agent decides to continue exploring the interior of the ROI. It is intentionally implemented as termination condition of the episodes in all the experiments of this paper. This ensures the same number of timesteps for the generated and reference tracks. By having a lower (big) bound on the number of timesteps (> 900) per episode, the bias from having variable horizon environments (Kostrikov et al., 2019) is then alleviated.

The state space of DATI may easily be enlarged to include more information such as destination of the trajectories — fixed in this work by the nature of the dataset. With this in mind, it could be used as a method of pathfinding for ocean voyages, given enough reference trajectories between source and destination. The advantage over modern methods which optimize for the shortest route (Rospotniuk & Small, 2022) is that DATI is data-driven, and therefore can learn (as part of the distribution) highly dynamic shipping patterns often encountered in reality, which may deviate from the shortest route, due to many varying external factors (Zygouras et al., 2021).

From normal to abnormal motion patterns. We leave for a different paper how to deal with multimodal distributions of trajectories. For the proof of concept of this work, we then restrict to the analysis of abnormal patterns in the 143 trajectories $s_{0:T}^*$ belonging to the cluster *other*, which start near the entrance to the golf of Mexico. DATI is run for each corresponding initial state, and $D_{\text{dtw}}(\hat{s}_{0:T}^\theta, s_{0:T}^*)$ is calculated and normalized with respect to the maximum value. We then ask for a threshold Λ for which about 10% of the trajectories are tagged as abnormal by setting $D_{\text{dtw}}(\hat{s}_{0:T}^\theta, s_{0:T}^*) > \Lambda$. This is obtained to be $\Lambda = 0.75$, and the corresponding trajectories are shown in red in Fig. 5(c). Independently, about 10% of the most salient anomalies in the test set are manually annotated and confronted with the predictions by DATI, resulting in a weighted F1-score of 0.78. This is very promising, given that the DATI architecture was chosen to optimize the synthetic experiments.

7. Conclusion and outlook

We have presented a novel method to learn representative trajectories of dynamical systems for which partial information of their update rule is known. The method does not make any assumption regarding the state representation, making it very appealing for knowledge discovery across a wide range of applications. We have demonstrated this by learning to generate representative trajectories in maritime traffic (with corresponding anomaly detection) with the same model architecture and hyperparameters with which we benchmarked the performance on synthetic datasets. Future research avenues within the trajectory data mining field include (but are not limited to) the detection of abnormal motion in more complex maritime scenarios with multi-modal distributions, in road and air traffic, pedestrian dynamics, etc. By providing a reinforcement learning environment capable of representing any family of trajectories, we encourage the research community to use a standard benchmark for trajectory imitation tasks.

Appendix A.

A.1 Shape parameters of synthetic families

For all families of trajectories we take $T = 2\pi/\omega$. The parameter set for each family is as follows. *FixedStart* has $\alpha = \{\alpha, \omega, \eta\}$ for which $\omega = \eta = 0.9$ are fixed and α is sampled uniformly in $[5, 10]$ for each episode. *UShaped* has $\alpha = \{\alpha, \omega\}$ for which $\omega = 0.9$ is fixed and α is sampled uniformly in $[0.2, 0.8]$ for each episode. *Circles* has $\alpha = \{\alpha, \omega\}$ for which $\omega = 0.4$ is fixed and α is sampled uniformly in $[0.5, 1.0]$ for each episode. *Ribbons* has $\alpha = \{\alpha, \omega, R_1, R_2\}$ for which $\omega = 0.4$, $R_1 = 1$, $R_2 = 2$ are fixed and α is sampled uniformly in $[-\pi, \pi]$ for each episode.

A.2 Hyperparameters for the synthetic experiments

DATI updates the critic networks 5 times before updating the actor networks per training batch. The learning rates for the actors is 10^{-4} , and for the critics 10^{-5} . They are optimized using Adam with $\beta_1 = 0.5$ and $\beta_2 = 0.9$. All L_1 losses are optimized with a learning rate of 10^{-3} and weighted (with respect to the total loss) with a coefficient of 10. The 1-Lipschitz condition for the critics is achieved by gradient penalty (Gulrajani et al., 2017) with $\lambda = 10$.

Finally, the noise η_t is chosen as the best between Ornstein-Uhlenbeck or Gaussian (with $\mu = 0$ and $\sigma = 0.3$). DDPG-TI optimizes the actor and critic networks using Adam with learning rates 10^{-4} and 2×10^{-4} , respectively. The discount factor is $\gamma = 0.9$ and the rate of update of the target networks is 10^{-3} . BC optimizes the networks using Adam with a learning rate 10^{-3} . The maximum likelihood procedure searches for a distribution with maximum entropy, the latter condition weighted with a coefficient of 10^{-3} . Exponential smoothing of D_{dtw} is done with a smoothing factor of 0.9.

A.3 Update equation for vessel motion

Given a path of length d on the surface of the Earth, connecting the points with geographical coordinates (λ_1, φ_1) and (λ_2, φ_2) — with $(\lambda, \varphi) = (\text{longitude}, \text{latitude})$ — the angle θ subtended by the path is related to the Earth radius as $\theta = d/R$. The haversine of θ is defined as $\text{hav}(\theta) \equiv \sin^2(\theta/2)$ and obeys

$$\text{hav}(\theta) = \text{hav}(\varphi_2 - \varphi_1) + \cos(\varphi_1) \cos(\varphi_2) \text{hav}(\lambda_2 - \lambda_1). \quad (9)$$

For small travelled distances $d/R \ll 1$ and $\Delta\varphi \equiv \varphi_2 - \varphi_1 \ll 1$ and $\Delta\lambda \equiv \lambda_2 - \lambda_1 \ll 1$. In this limit, (9) becomes, after Taylor expansion,

$$(d/R)^2 = \Delta\varphi^2 + \cos^2(\varphi_1) \Delta\lambda^2. \quad (10)$$

This expresses how the curved geometry on a sphere looks locally flat (i.e. Euclidean) as long as the axis of λ is rescaled with $\cos(\varphi_1)$. With COG representing the angle along which the vessel moves (with respect to the geographical North), and SOG Δt the small distance travelled during Δt

$$\begin{aligned} \Delta\varphi &= \frac{1}{60} \cos(\text{COG}) \text{SOG } \Delta t \\ \cos(\varphi_1) \Delta\lambda &= \frac{1}{60} \sin(\text{COG}) \text{SOG } \Delta t, \end{aligned} \quad (11)$$

where the factor $\frac{1}{60}$ is used to convert from knots to degrees: $[\text{SOG}] = 1 \text{ knot} = 1 \text{ nmi/hour}$ and $60 \text{ nmi} \sim 1^\circ$ of longitude / latitude (i.e. The equatorial earth radius is $R = 6378.137 \text{ km}$ so, with $\theta = \pi \text{ rad}/180$, $d = 6378.14 * \pi / 180 \text{ km} = 111.319 \text{ km} = \underline{60.1 \text{ nmi}}$. On the other hand, the polar radius is $R = 6356.752 \text{ km}$ so $d = 6356.752 * \pi / 180 \text{ km} = 110.946 \text{ km} = \underline{59.9 \text{ nmi}}$).

References

- Agarwal, R., Schwarzer, M., Castro, P. S., Courville, A., & Bellemare, M. G. (2021). Deep reinforcement learning at the edge of the statistical precipice. In *Thirty-Fifth Conference on Neural Information Processing Systems*.
- Arjovsky, M., Chintala, S., & Bottou, L. (2017). Wasserstein generative adversarial networks. In *Proceedings of the 34th International Conference on Machine Learning*, pp. 214–223.
- Arulkumaran, K., Deisenroth, M. P., Brundage, M., & Bharath, A. A. (2017). Deep reinforcement learning: A brief survey. *IEEE Signal Processing Magazine*, 34(6), 26–38.
- Bay, S. M. (2017). Evaluation of factors on the patterns of ship movement and predictability of future ship location in the gulf of mexico..

- Becker-Ehmck, P., Karl, M., Peters, J., & van der Smagt, P. (2020). Learning to fly via deep model-based reinforcement learning. *CoRR*, *abs/2003.08876*.
- Belhadi, A., Djenouri, Y., Lin, J. C.-W., & Cano, A. (2020). Trajectory outlier detection: Algorithms, taxonomies, evaluation, and open challenges.. *11*(3).
- Brockman, G., Cheung, V., Pettersson, L., Schneider, J., Schulman, J., Tang, J., & Zaremba, W. (2016). Openai gym. *arXiv preprint arXiv:1606.01540*.
- Chen, P., & Lu, W. (2021). Deep reinforcement learning based moving object grasping. *Information Sciences*, *565*, 62–76.
- Choi, S., Kim, S., & Jin Kim, H. (2017). Inverse reinforcement learning control for trajectory tracking of a multirotor uav. *International Journal of Control, Automation and Systems*, *15*(4), 1826–1834.
- Durall, R., Chatzimichailidis, A., Labus, P., & Keuper, J. (2021). Combating mode collapse in gan training: An empirical analysis using hessian eigenvalues. In *VISIGRAPP*.
- Freeman, C., Merriman, J., Beaver, I., & Mueen, A. (2022). Experimental comparison and survey of twelve time series anomaly detection algorithms. *J. Artif. Int. Res.*, *72*, 849–899.
- Giannotti, F., Nanni, M., & Pedreschi, D. (2006). Efficient mining of temporally annotated sequences. In *In Proceedings of the 6th SIAM International Conference on Data Mining*, pp. 346–357.
- Giannotti, F., Nanni, M., Pinelli, F., & Pedreschi, D. (2007). Trajectory pattern mining.. *KDD '07*, p. 330–339, New York, NY, USA. Association for Computing Machinery.
- Goodfellow, I. J. (2017). NIPS 2016 tutorial: Generative adversarial networks. *CoRR*, *abs/1701.00160*.
- Gulrajani, I., Ahmed, F., Arjovsky, M., Dumoulin, V., & Courville, A. C. (2017). Improved training of wasserstein gans. In *Advances in Neural Information Processing Systems*, Vol. 30.
- Haarnoja, T., Zhou, A., Ha, S., Tan, J., Tucker, G., & Levine, S. (2019). Learning to walk via deep reinforcement learning. In *Robotics: Science and Systems*.
- Hafner, R., Hertweck, T., Kloppner, P., Bloesch, M., Neunert, M., Wulfmeier, M., Tunyasuvunakool, S., Heess, N. M. O., & Riedmiller, M. A. (2020). Towards general and autonomous learning of core skills: A case study in locomotion. In *CoRL*.
- Kazemi, S. M., Goel, R., Eghbali, S., Ramanan, J., Sahota, J., Thakur, S., Wu, S., Smyth, C., Poupart, P., & Brubaker, M. (2019). Time2vec: Learning a vector representation of time. *CoRR*, *abs/1907.05321*.
- Kim, K., Gu, Y., Song, J., Zhao, S., & Ermon, S. (2020). Domain adaptive imitation learning. In III, H. D., & Singh, A. (Eds.), *Proceedings of the 37th International Conference on Machine Learning*, Vol. 119 of *Proceedings of Machine Learning Research*, pp. 5286–5295. PMLR.
- Kontopoulos, I., Makris, A., Zissis, D., & Tserpes, K. (2021). A computer vision approach for trajectory classification. In *2021 22nd IEEE International Conference on Mobile Data Management (MDM)*, pp. 163–168.

- Kostrikov, I., Agrawal, K. K., Dwibedi, D., Levine, S., & Tompson, J. (2019). Discriminator-actor-critic: Addressing sample inefficiency and reward bias in adversarial imitation learning. In *ICLR*.
- Last, P., Bahlke, C., Hering-Bertram, M., & Linsen, L. (2014). Comprehensive analysis of automatic identification system (ais) data in regard to vessel movement prediction. *Journal of Navigation*, 67(5), 791–809.
- Lazaridis, A., Fachantidis, A., & Vlahavas, I. P. (2020). Deep reinforcement learning: A state-of-the-art walkthrough. *J. Artif. Intell. Res.*, 69, 1421–1471.
- Lee, H., & Kim, H. J. (2017). Trajectory tracking control of multirotors from modelling to experiments: A survey. *International Journal of Control, Automation and Systems*, 15(1), 281–292.
- Lee, S., Park, M., Lee, K., & Lee, J. (2019). Scalable muscle-actuated human simulation and control. *ACM Trans. Graph.*, 38(4).
- Li, Z., Ding, B., Han, J., Kays, R., & Nye, P. (2010). Mining periodic behaviors for moving objects.. KDD '10, p. 1099–1108, New York, NY, USA. Association for Computing Machinery.
- Li, Z., Han, J., Ding, B., & Kays, R. (2012). Mining periodic behaviors of object movements for animal and biological sustainability studies. *Data Mining and Knowledge Discovery*, 24(2), 355–386.
- Lillicrap, T. P., Hunt, J. J., Pritzel, A., Heess, N., Erez, T., Tassa, Y., Silver, D., & Wierstra, D. (2016). Proceedings of the 4th international conference of learning representation (iclr). In *Continuous Control with Deep Reinforcement Learning*.
- Liu, L., & Hodgins, J. (2018). Learning basketball dribbling skills using trajectory optimization and deep reinforcement learning. *ACM Trans. Graph.*, 37(4).
- Meng, F., Yuan, G., Lv, S., Wang, Z., & Xia, S. (2019). An overview on trajectory outlier detection. *Artificial Intelligence Review*, 52(4), 2437–2456.
- Oh, M.-h., & Iyengar, G. (2019). Sequential anomaly detection using inverse reinforcement learning.. KDD '19, p. 1480–1490, New York, NY, USA. Association for Computing Machinery.
- Peng, X. B., Coumans, E., Zhang, T., Lee, T.-W. E., Tan, J., & Levine, S. (2020). Learning agile robotic locomotion skills by imitating animals. In *Robotics: Science and Systems*.
- Peng, X. B., Kanazawa, A., Malik, J., Abbeel, P., & Levine, S. (2018). Sfv: Reinforcement learning of physical skills from videos. *ACM Trans. Graph.*, 37(6).
- Pomerleau, D. A. (1991). Efficient training of artificial neural networks for autonomous navigation. *Neural Computation*, 3(1), 88–97.
- Raychaudhuri, D. S., Paul, S., van Baar, J., & Roy-Chowdhury, A. K. (2021). Cross-domain imitation from observations. *CoRR*, abs/2105.10037.
- Reddy, S., Dragan, A. D., & Levine, S. (2020). Sqil: Imitation learning via reinforcement learning with sparse rewards. In *8th International Conference on Learning Representations (ICLR)*.

- Roses, R., Kadar, C., Gerritsen, C., & Rouly, O. C. (2020). Simulating offender mobility: Modeling activity nodes from large-scale human activity data. *J. Artif. Intell. Res.*, 68, 541–570.
- Rospotniuk, V., & Small, R. (2022). Optimal any-angle pathfinding on a sphere. *J. Artif. Int. Res.*, 72, 475–505.
- Ross, S., & Bagnell, D. (2010). Efficient reductions for imitation learning. In *Proceedings of the Thirteenth International Conference on Artificial Intelligence and Statistics*, Vol. 9, pp. 661–668.
- Rubi, B., Morcego, B., & Perez, R. (2021a). Deep reinforcement learning for quadrotor path following with adaptive velocity. *Autonomous Robots*, 45(1), 119–134.
- Rubi, B., Morcego, B., & Perez, R. (2021b). Quadrotor path following and reactive obstacle avoidance with deep reinforcement learning. *Journal of Intelligent & Robotic Systems*, 103(4), 62.
- Rubi, B., Perez, R., & Morcego, B. (2020). A survey of path following control strategies for uavs focused on quadrotors. *Journal of Intelligent and Robotic Systems*, 98(2), 241–265.
- Salvador, S., & Chan, P. K.-F. (2004). Fastdtw: Toward accurate dynamic time warping in linear time and space..
- Solano-Carrillo, E., Carrillo-Perez, B., Flenker, T., Steiniger, Y., & Stoppe, J. (2021). Detection and geovisualization of abnormal vessel behavior from video. In *2021 IEEE International Intelligent Transportation Systems Conference (ITSC)*, pp. 2193–2199.
- Wang, D., Miwa, T., & Morikawa, T. (2020a). Big trajectory data mining: A survey of methods, applications, and services..
- Wang, S., Toyer, S., Gleave, A., & Emmons, S. (2020b). The imitation library for imitation learning and inverse reinforcement learning. <https://github.com/HumanCompatibleAI/imitation>.
- Xue, W., Kolaric, P., Fan, J., Lian, B., Chai, T., & Lewis, F. L. (2021a). Inverse reinforcement learning in tracking control based on inverse optimal control. *IEEE Transactions on Cybernetics*, 1–12.
- Xue, W., Lian, B., Fan, J., Kolaric, P., Chai, T., & Lewis, F. L. (2021b). Inverse reinforcement q-learning through expert imitation for discrete-time systems. *IEEE Transactions on Neural Networks and Learning Systems*, 1–14.
- Young, B. L. (2017). Predicting vessel trajectories from ais data using r..
- Zheng, B., Verma, S., Zhou, J., Tsang, I. W., & Chen, F. (2021). Imitation learning: Progress, taxonomies and opportunities. *CoRR*, abs/2106.12177.
- Zheng, Y. (2015). Trajectory data mining: An overview. *ACM Trans. Intell. Syst. Technol.*, 6(3).
- Zhu, J., Park, T., Isola, P., & Efros, A. A. (2017). Unpaired image-to-image translation using cycle-consistent adversarial networks. In *International Conference on Computer Vision*.

Zygouras, N., Spiliopoulos, G., & Zissis, D. (2021). Detecting representative trajectories from global ais datasets. In *2021 IEEE International Intelligent Transportation Systems Conference (ITSC)*, pp. 2278–2285.